

- **Introduction to Pulse Shape Analysis (PSA) -**
- **Basis Generation -**
- Coincidence and Pulse Shape Comparison based Scan (PSCS) -

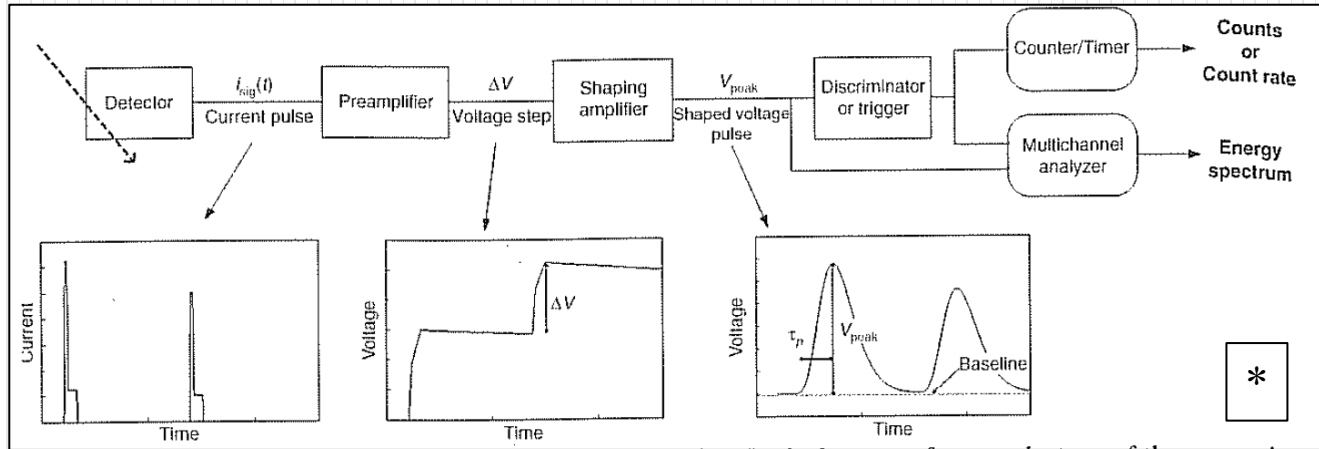
**Fabio Crespi**  
**Università di Milano - INFN**

# Outline

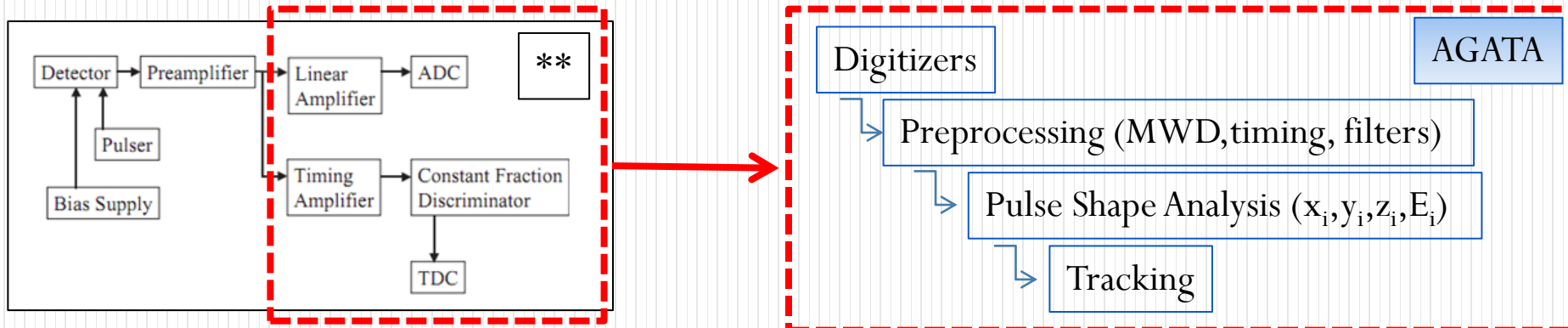
- **Introduction to Pulse Shape Analysis**
  - PSA with HPGe detectors
  - Current pulse shape formation process
  - Factors limiting the extraction of information from the signal shape
  - Examples of useful information extracted using PSA techniques
  - PSA with gamma-ray tracking array AGATA
    - The PSA problem
    - Grid Search Algorithm
    - AGATA PSA performances
    - Signal Decomposition in Single hit/multiple hits case
- **Basis Generation**
  - PSA and signal basis ( calculated / experimental signals )
  - The case of 24-fold segmented cylindrical HPGe detector
  - Spatial sensitivity of detectors

# Introduction to Pulse Shape Analysis (PSA)

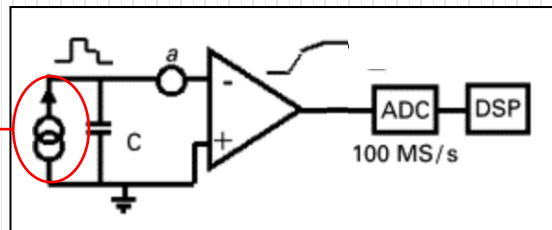
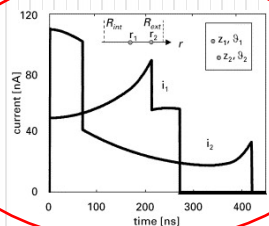
## Pulse Height Analysis



## Analog → Digital



## Pulse Shape Analysis (Digital / Analog)



\*G.F. Knoll, Radiation Detection and Measurement, second ed., Wiley, New York, 1989.

\*\* "Developments in large gamma-ray detector arrays", I Y Lee *et al* 2003 *Rep. Prog. Phys.* **66** 1095.

\*\*\* "Spatial localization of multiple simultaneous hits in segmented HPG detectors: a new algorithm", E. Gatti *et al* NIMA 458 (2001) 738

# Introduction to Pulse Shape Analysis

$$Q(t) = Q^-(t) + Q^+(t) \quad *$$

$$Q^+(t) = \frac{q_0 \alpha}{V_0} [r_0^2 - r_h^2(t)] + \frac{q_0 \beta}{V_0} \ln \frac{r_0}{r_h(t)}$$

$$Q^-(t) = \frac{\Delta E^-}{V_0} = \frac{q_0 \alpha}{V_0} [r_e^2(t) - r_0^2] + \frac{q_0 \beta}{V_0} \ln \frac{r_e(t)}{r_0}$$

$$\alpha \equiv \frac{eN_A}{4\epsilon} \quad \beta \equiv \frac{V_0 - \alpha(r_2^2 - r_1^2)}{\ln(r_2 / r_1)}$$

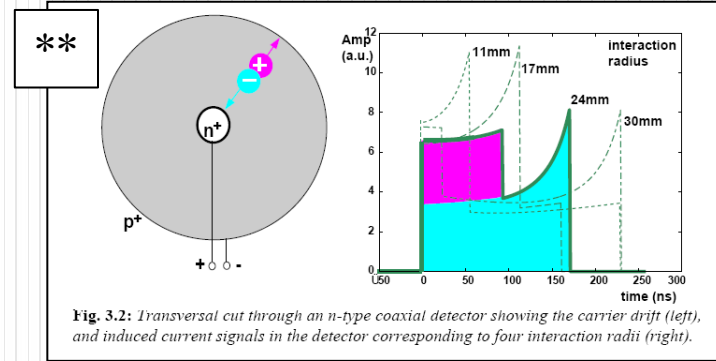
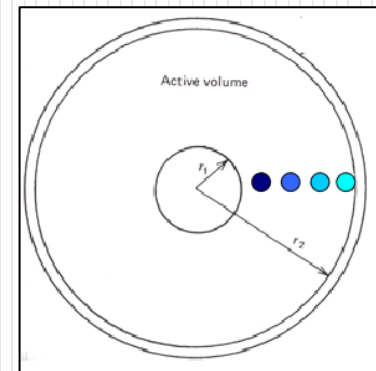
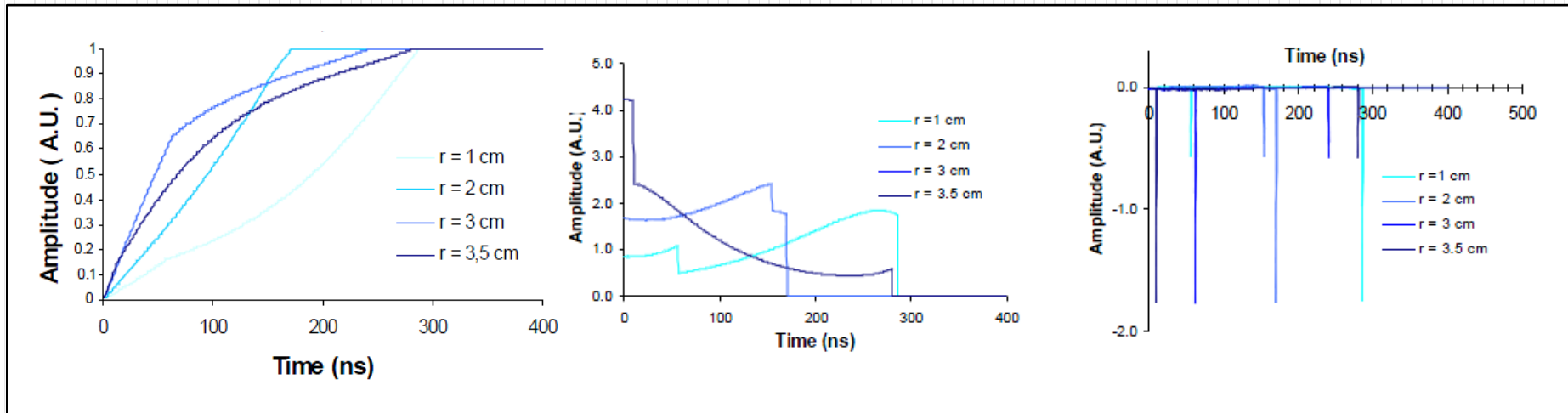


Fig. 3.2: Transversal cut through an n-type coaxial detector showing the carrier drift (left), and induced current signals in the detector corresponding to four interaction radii (right).

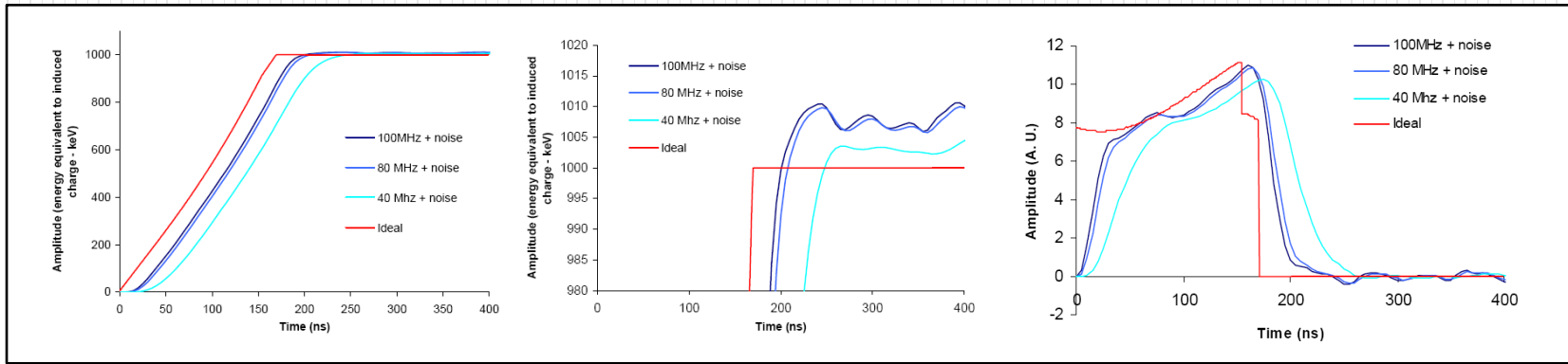


\*G.F. Knoll, Radiation Detection and Measurement, second ed., Wiley, New York, 1989.

\*\* J. Gerl, W. Korten (Eds.), AGATA Technical Proposal, September 2001, available at <http://www-win.gsi.de/agata/>



## Factors limiting the extraction of information from the signal shape



Charge signals, represented in equivalent amount of energy released, are shown. In the right panels the correspondent current pulses are displayed. The simulated event is relative to a total energy deposit of 500 keV, with two IPs inside one detector segment. The **ideal case** (upper panels) and a **realistic one**, where the frequency cut of the preamplifier, the electric noise and a digital filtering have been applied.

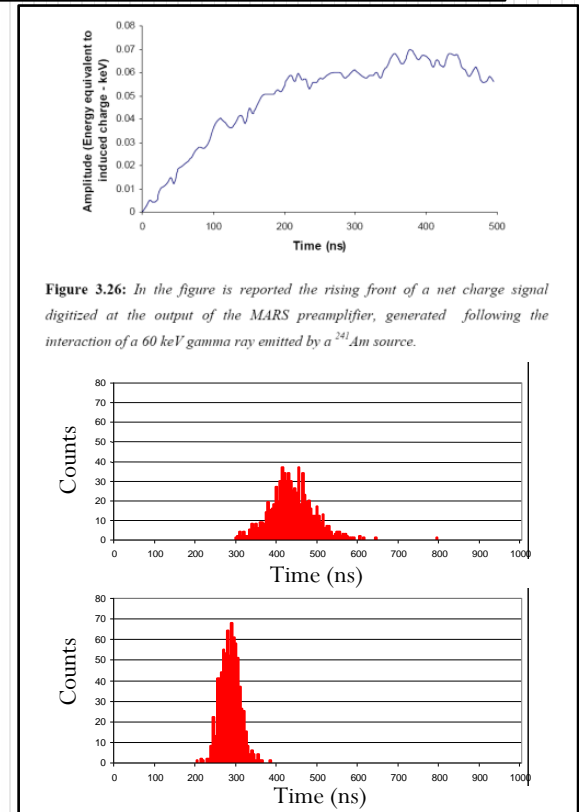
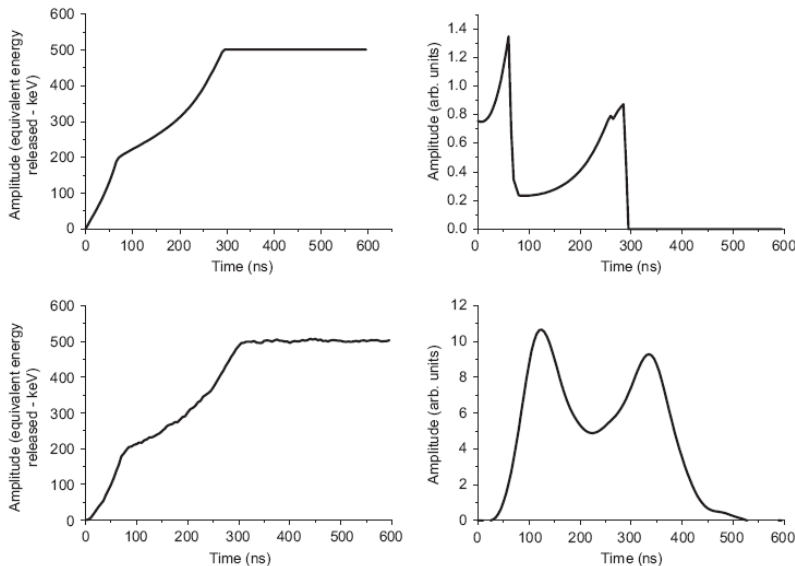


**Figure 3.26:** In the figure is reported the rising front of a net charge signal digitized at the output of the MARS preamplifier, generated following the interaction of a 60 keV gamma ray emitted by a  $^{241}\text{Am}$  source.

\*"A pulse shape analysis algorithm for HPGe detectors" F.C.L. Crespi, Nucl. Instr. and Meth. A 570 (2007) 459.

## Examples of some useful information extracted using PSA techniques

### Spatial localization of interactions

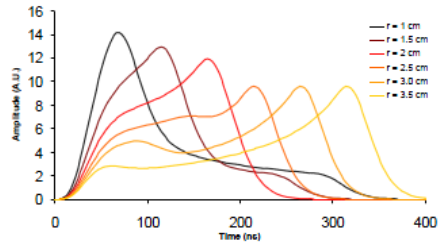


Figure 3.10a: Current pulse shapes for interactions with different radial position inside a non segmented cylindrical HPGe detector. The signals are calculated on the base of relations (3.2) and the effect of electronic chain components response has been taken into account. In particular the simulated sampling frequency is 40 MHz.

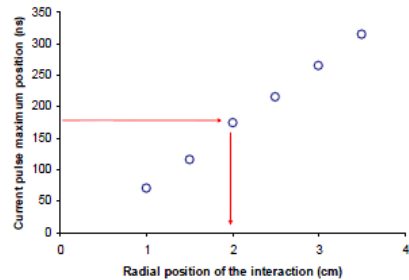


Figure 3.10b: The position of the current pulse maximum of the signals in figure 3.10a is plotted versus the radial position of the interaction, it is clear that there is a direct correspondence between the two quantities. As is shown by the arrows it is possible to deduce the radial coordinate by measuring the current pulse maximum.

“Background reduction and sensitivity for germanium double beta decay experiments”, Gómez, H. 2007 *Astroparticle Physics* 28 (4-5), pp. 435-447

\*\*G.F. Knoll, Radiation Detection and Measurement, second ed., Wiley, New York, 1989.

\*\*\* \*\*”A pulse shape analysis algorithm for HPGe detectors” F.C.L. Crespi, Nucl. Instr. and Meth. A 570 (2007) 459.

### Number of interaction sites

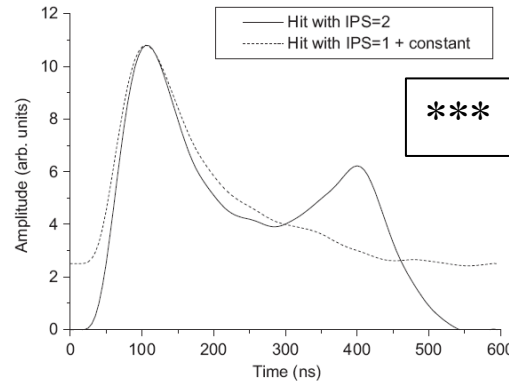
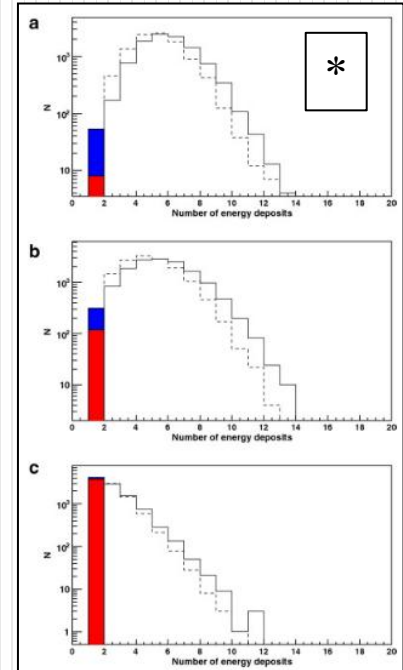


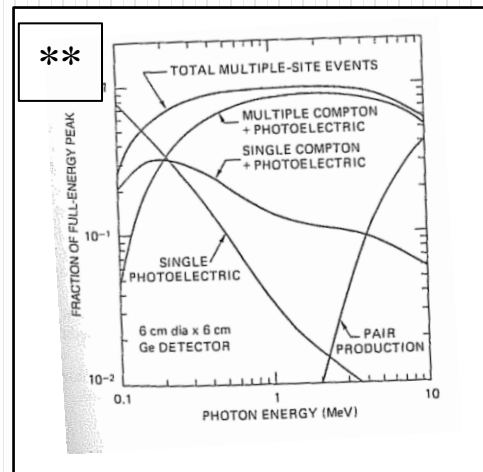
Fig. 4. The current signal produced by an event with two IPs is indicated with the continuous line. The first hit has deposited 60% of the total energy at  $R = 3.5$  cm,  $\theta = 20^\circ$  and  $z = 0$ . The second IP has been positioned at  $R = 0.6$  cm with the same  $\theta$  and  $z$ . With the dashed line, the event relative to the first IP plus a constant is plotted.

### Background Suppression



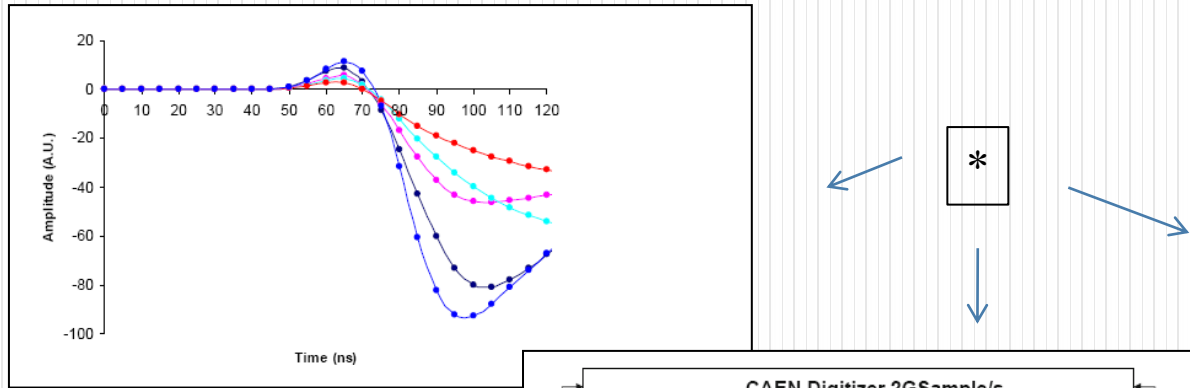
‘Distribution of the number of energy deposits per event in the 2–2.1 MeV RoI for all the background contributions studied:  $^{60}\text{Co}$  (a),  $^{68}\text{Ge}$  (b) and 2614.5 keV photons (c), for 4-kg detector and considering a spatial resolution of 3 (solid line) and 5 mm (dashed line). Monosite events are singled out in red (blue) for 3 (5) mm resolution.’\*

### Improved quality of gamma spectra



## Introduction to Pulse Shape Analysis

- Pulse Shape Analysis has been used to improve the time resolution of HighPurity Germanium (HPGe) detectors.
- Time aligned signals were acquired in a coincidence measurement using a coaxial HPGe and a cerium-doped lanthanum chloride (LaCl<sub>3</sub>:Ce) scintillation detector.
- The analysis using a Constant Fraction Discriminator (CFD) time output versus the HPGe signal shape shows that time resolution ranges from 2 to 12 ns depending on the slope in the initial part of the signal.



\*"HPGe detectors timing using pulse shape analysis techniques" F.C.L. Crespi, Nucl. Instr. and Meth. A 610 (2010) 299.

\*\*M. Moszynski, B. Bengtson, Application of pulse shape selection method to a true coaxial Ge(Li) detector for measurements of nanosecond half-lives, Nucl. Instr. and Meth. 80 (1970) 233.

\*\*\*B. Bengtson, M. Moszynski, Subnanosecond timing with a planar Ge(Li) detector, Nucl. Instr. and Meth. 100 (1972) 293.

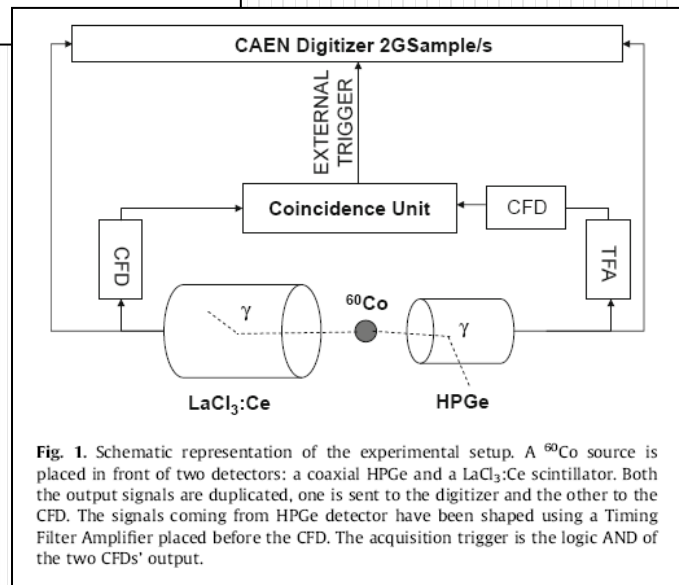


**Fig. 1.** Schematic representation of the experimental setup. A <sup>60</sup>Co source is placed in front of two detectors: a coaxial HPGe and a LaCl<sub>3</sub>:Ce scintillator. Both the output signals are duplicated, one is sent to the digitizer and the other to the CFD. The signals coming from HPGe detector have been shaped using a Timing Filter Amplifier placed before the CFD. The acquisition trigger is the logic AND of the two CFDs' output.

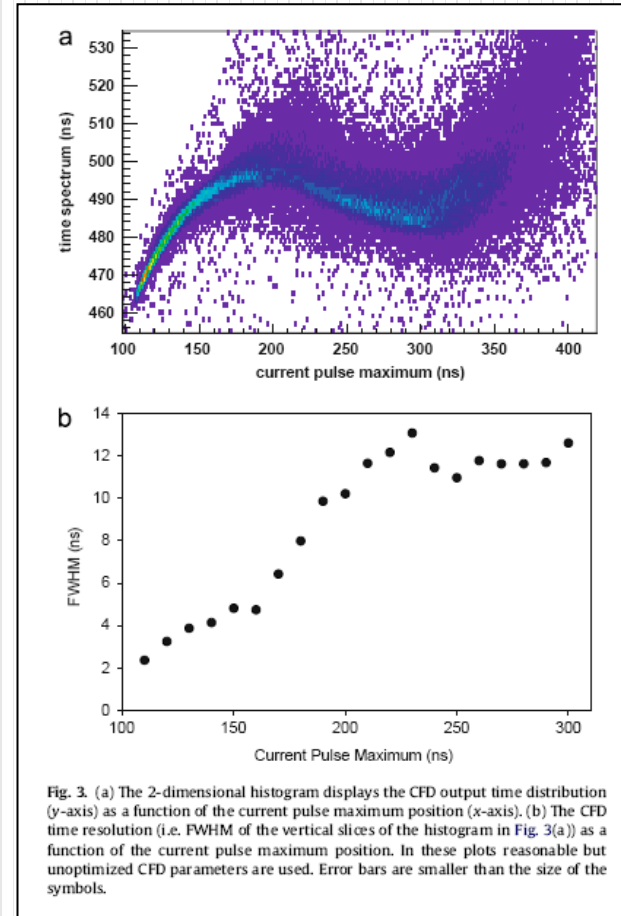


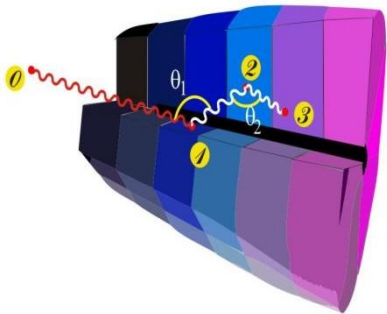
**Fig. 3.** (a) The 2-dimensional histogram displays the CFD output time distribution (y-axis) as a function of the current pulse maximum position (x-axis). (b) The CFD time resolution (i.e. FWHM of the vertical slices of the histogram in Fig. 3(a)) as a function of the current pulse maximum position. In these plots reasonable but unoptimized CFD parameters are used. Error bars are smaller than the size of the symbols.

3D localization of interaction sites → segmented HPGe detectors

# Ingredients of Gamma Tracking

1

Highly segmented  
HPGe detectors



2

Digital electronics  
to record and  
process segment signals



Identified  
interaction points

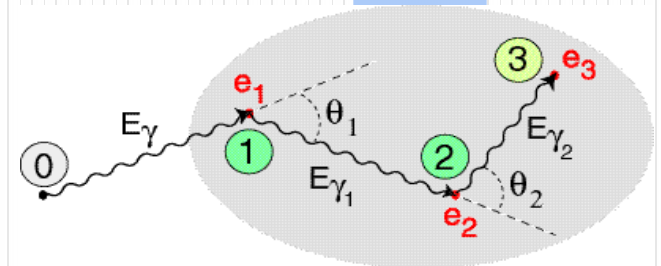
$$(x, y, z, E, t)_i$$

Pulse Shape Analysis  
to decompose  
recorded waves

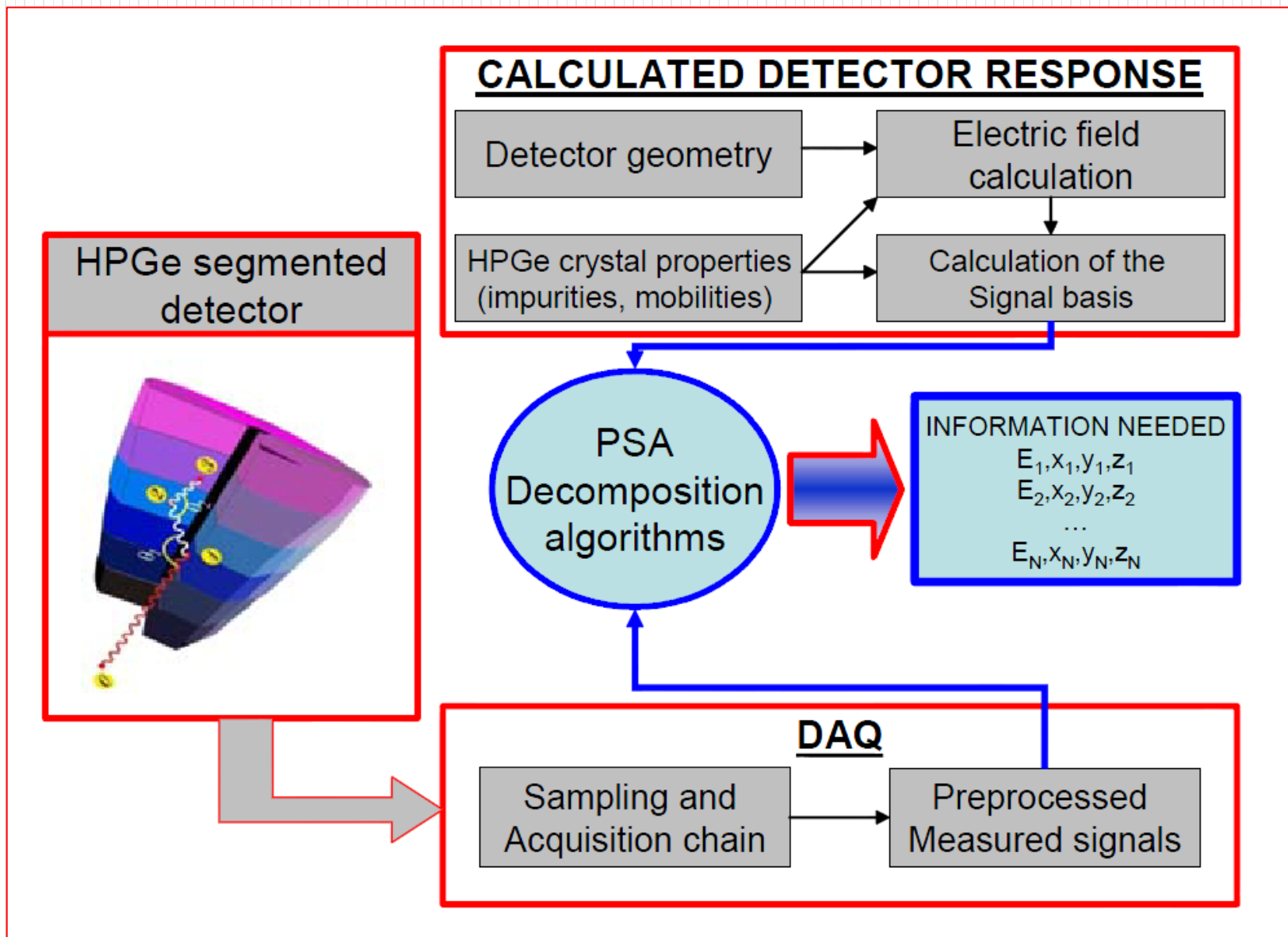
3

4

Reconstruction of tracks  
evaluating permutations  
of interaction points



Reconstructed  
gamma-rays



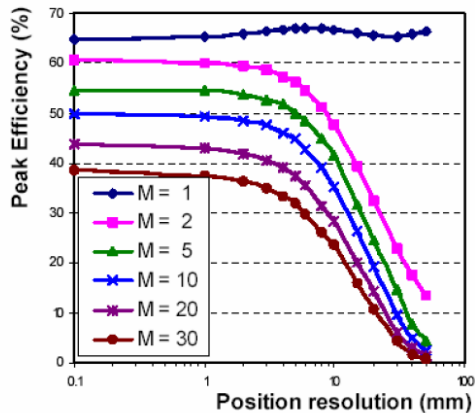
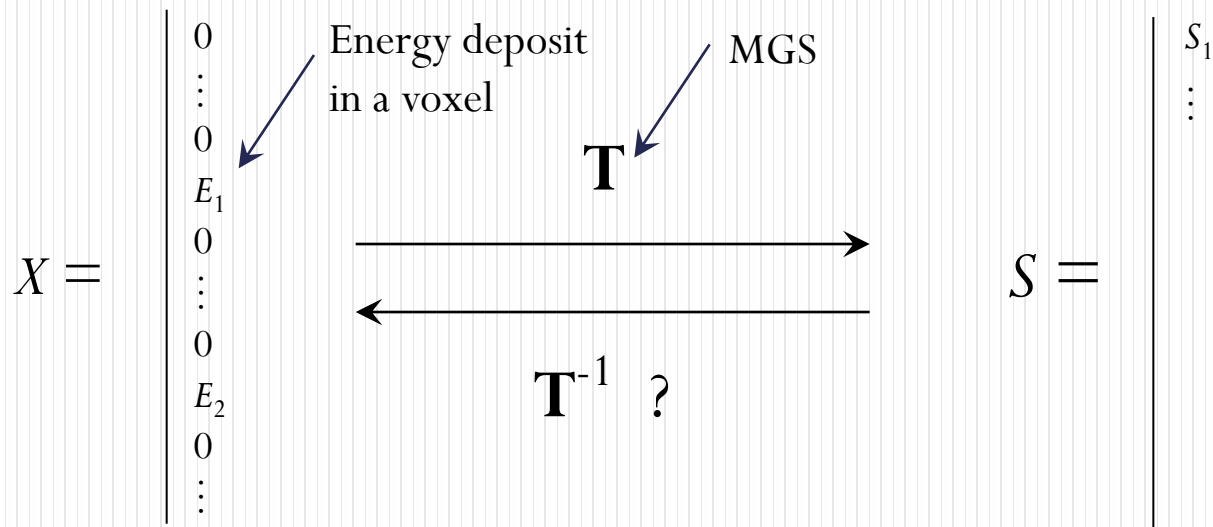


**Figure 3.1:** The total peak efficiency of “cluster-tracking” reconstructed data is shown as a function of assumed position resolution and  $\gamma$ -ray multiplicity [79].

\*” A. Olariou, P. Desesquelles, et al., IEEE Trans. Nucl. Sci. NS53 (1) (2006) 1028.

\*\* P. Desesquelles presentations at the AGATA weeks (e.g. GSI, February 2005) available at <http://www-win.gsi.de/agata/>

## The “PSA problem” in AGATA

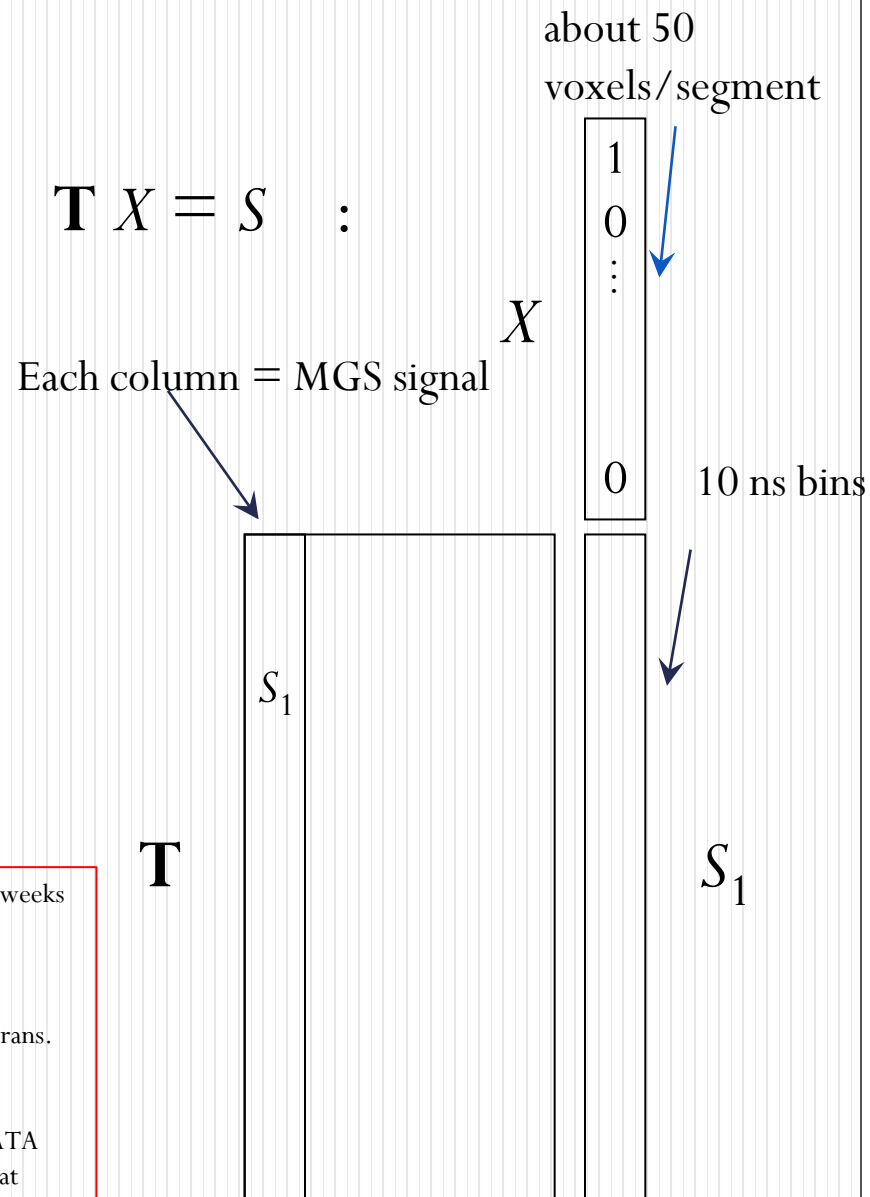


- Full “Least Squares” matrix is underdetermined (singular).
- can be decomposed into the product of three matrices, one of which contains the correlations (eigenvalues). By neglecting the small eigenvalues, the product can be inverted.
- Then an approximate fit can be obtained with very little computational effort, using a precalculated SVD inverse.
- The more eigenvalues kept, the higher the quality of the fit.

\* D. C. Radford presentations at the AGATA weeks (e.g. GSI, February 2005) available at at <http://www-win.gsi.de/agata/>

\*\* A. Olariou, P. Desesquelles, et al., IEEE Trans. Nucl. Sci. NS53 (1) (2006) 1028.

\*\*\* P. Desesquelles presentations at the AGATA weeks (e.g. GSI, February 2005) available at at <http://www-win.gsi.de/agata/>



## ADAPTIVE GRID SEARCH

\*

Roberto Venturelli  
INFN Padova - IPSIA "Giorgi" Verona

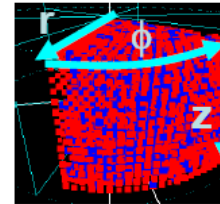
### SEARCH THE BEST $\chi^2$ FOR PULSE SHAPES IN THE REFERENCE BASE

Two possibilities:

#### SEARCH 1 POINT IN THE SEGMENT

Hypothesis: in case of multiple hits in segment the energetic barycentre is considered

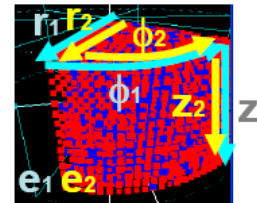
r-phi-z cycle in a coarse grid inside the real segment  
r-phi-z cycle with the fine grid in a small volume identified



#### SEARCH 2 POINTS IN THE SEGMENT

Hypothesis: in case of multiple hits in segment at most two points are considered

e energy division cycle  
(r-phi-z)<sub>1</sub> (r-phi-z)<sub>2</sub> cycle in a coarse grid  
(r-phi-z)<sub>1</sub> (r-phi-z)<sub>2</sub> cycle in a small volume with the fine grid



**Events with more than one net charge segment, are split into “independent” subevents → no combined search → scales linearly with segment multiplicity**

- When two points have similar energy there is a high probability to make a mistake in position assignment (position exchange)
- When two points have very different energy, the one with higher energy is well identified in position but the other can be everywhere (high uncertainty)
- The two analyses have similar performances for our experimental data.
- The SEARCH ONE POINT is much faster
- Simulations say that Doppler correction and  $\gamma$ -ray tracking do not suffer too much from this assumption

\* R. Venturelli presentations at AGATA weeks (e.g. Liverpool June 2006) available at <http://www-win.gsi.de/agata/>

\*\* R. Venturelli, et al., LNL Annual Report 2002, INFN-LNL(REP)198/2003, pp. 154–156

# GRID SEARCH: the principle

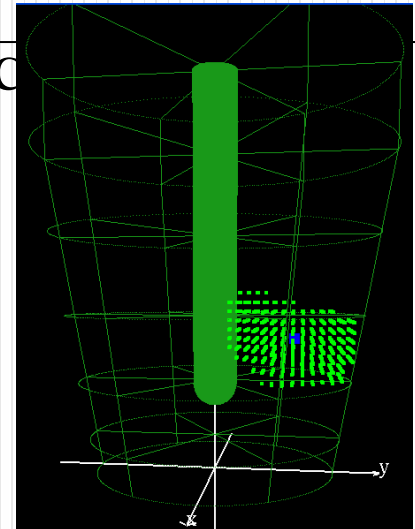
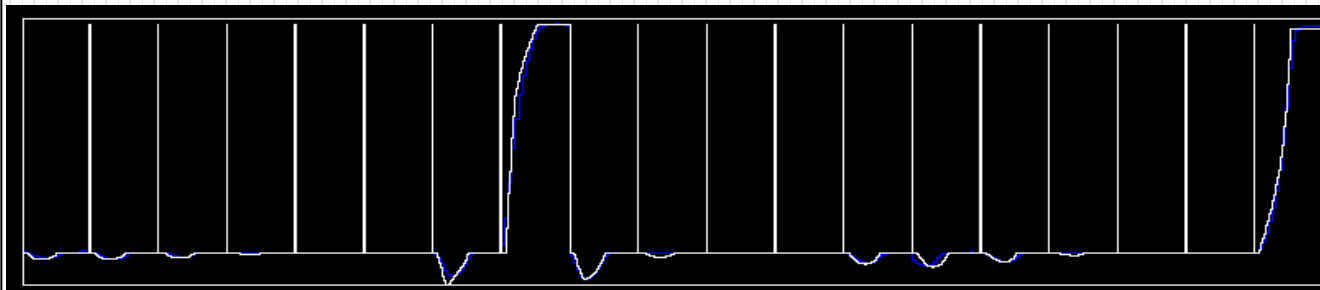
SEARCH THE BEST  $\chi^2$  FOR PULSE SHAPES IN THE REFERENCE

SEARCH 1 POINT IN THE SEGMENT  $[l]SEG\_GRID\_PTS:10^3$

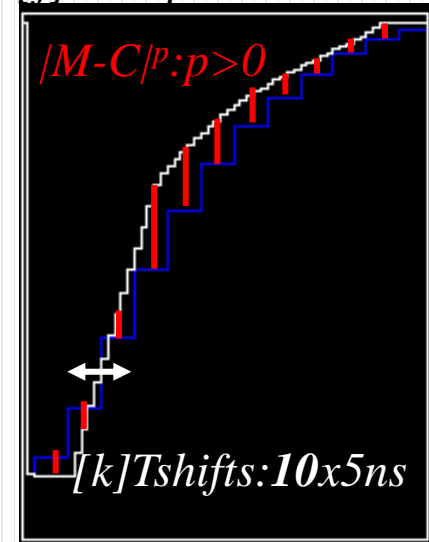
$$\chi_{\bar{l}, \bar{k}}^2 = \min_{\substack{l \in \{SEG\_GRID\_PTS\} \\ -Tshifts < k < Tshifts}} \left\{ \sum_i^{\substack{Tsamples \\ Signals}} \sum_j \left| M_i(j) - C_i^l(j+k) \right|^p \right\}$$

$$\left\{ x_{\bar{l}}, y_{\bar{l}}, z_{\bar{l}}, E_{hit}, \Delta t(\bar{k}) \right\}$$

$[i]Signals$ : TRANSIENTS, NET CHARGE, CORE (up to 37)



$[j]Tsamples: 25 \times 25 ns$



# GRID SEARCH: the principle

## MULTIPLE HITS PER SEGMENT

### SEARCH 2 POINTS IN THE SEGMENT

**Hypothesis:** in case of multiple hits in segment at most two points are considered

$$\{ \text{measuredSamples}, E_{\text{segm}} \}$$

$$\chi_{\bar{l}_1, \bar{l}_2, \bar{k}}^2 = \min_{\substack{l_1, l_2 \in \{SEG\_GRID\_PTS\} \\ -Tshifts < k < Tshifts \\ 0 < f < .5}} \left\{ \sum_j^{T_{\text{samples}} \text{ Signals}} \left| M_i(j) - [f \cdot C_i^{l_1}(j+k) + (1-f) \cdot C_i^{l_2}(j+k)] \right|^p \right\}$$

$$\{ x_{\bar{l}_1}, y_{\bar{l}_1}, z_{\bar{l}_1}, x_{\bar{l}_2}, y_{\bar{l}_2}, z_{\bar{l}_2}, E_{\text{segm}} \cdot f, E_{\text{segm}} \cdot (1-f), \Delta t(\bar{k}) \}$$

# Core of the program

- Just a sequence of loops with almost no calculations
- Runs fast because all structures fit in memory

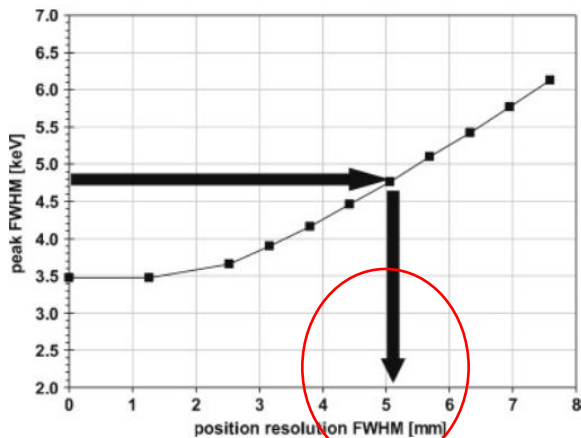
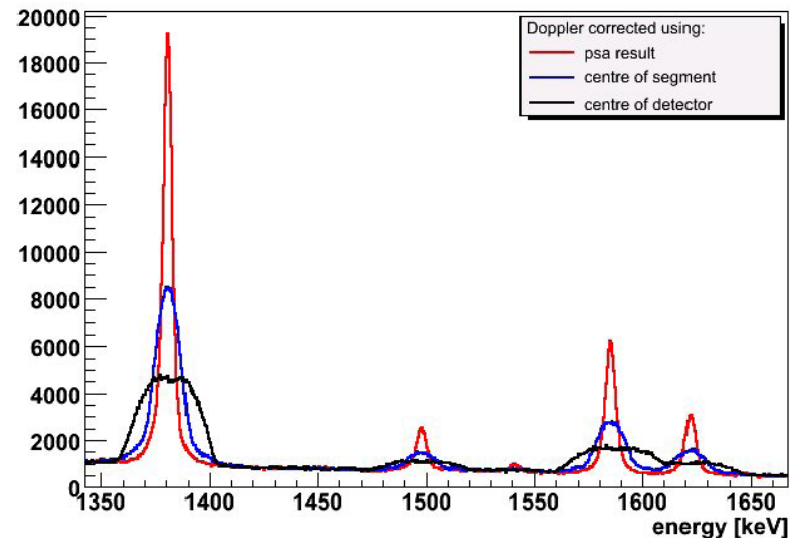
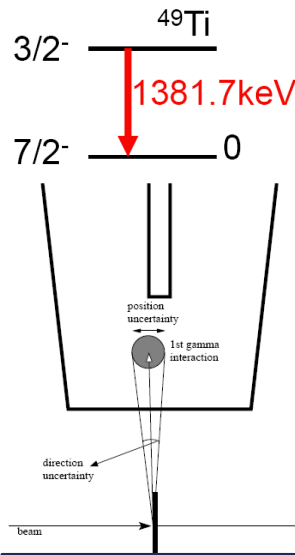
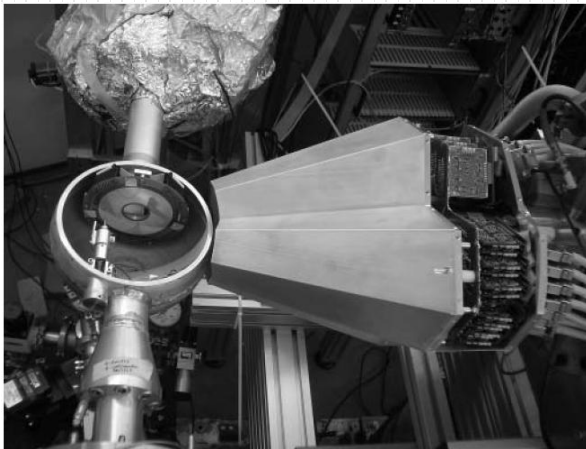
```
#define RERRE 24
#define RPHI 25
#define RZETA 60
#define RTIME 70
#define RSEGM 25

int amplitude[RERRE][RPHI][RZETA][RTIME][RSEGM]; //erre phi zeta time segment      252 MByte

chi2min=1000000000;
for(ierre=4;ierre<=RERRE;ierre+=step1A){
  for(iphi=1;(iphi <=2+ierre)&&(iphi<=RPHI) ;iphi+=step1A){
    for(izeta=zetar[slice][0];izeta<=zetar[slice][1];izeta+=step1A){
      for(dt=-rt;dt<=rt;dt++){
        for(itime=10, chi2=0; (itime<=RTIME-10) && (chi2<chi2min); itime+=step1B){
          for(kk=1; (kk<=segments[slice][0]) ;kk++){
            isegm=segments[slice][kk];
            aa=samples[itime-3+dt][isegm-1];
            bb=amplitude[ierre-1][iphi-1][izeta-1][itime-1][isegm-1];
            if (isegm==ref)
              chi2 += (long) (metrica[aa-bb+5000]/weights[mult-1]);
            else
              chi2 += metrica[aa-bb+5000];
          }
        }
        if(chi2<chi2min) {
          chi2min = chi2;
          erreb = ierre;
          phib = iphi;
          zetab = izeta;
          bestdt = dt;
        }
      }
    }
  }
}
```

\* R. Venturelli presentations at AGATA weeks (e.g. Liverpool June 2006) available at <http://www-win.gsi.de/agata/>

\*\* R. Venturelli, et al., LNL Annual Report 2002, INFN-LNL(REP)198/2003, pp. 154–156



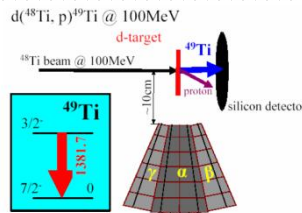
Width of the simulated 1382 keV peak as a function of the position smearing for the full triple cluster. Individual crystal energy resolution have been considered. All of the segment multiplicities are taken into account. The horizontal arrow indicates the experimental width.

- $^{48}\text{Ti}$  beam @100MeV
- 6.5% v/c
- deuterium target
- Inverse kinematics
- $^{48}\text{Ti}(d,p)^{49}\text{Ti}$

Performed at IKP  
Cologne

Aug-Sept 2005

3 Symmetric Prototype  
AGATA detectors  
Annular Si DSSSD



Doppler-corrected spectra for the full cluster, deducing the direction of the photon respectively from the centre of the detector, centre of the segment and from the PSA information. All of the segment multiplicities have been considered.

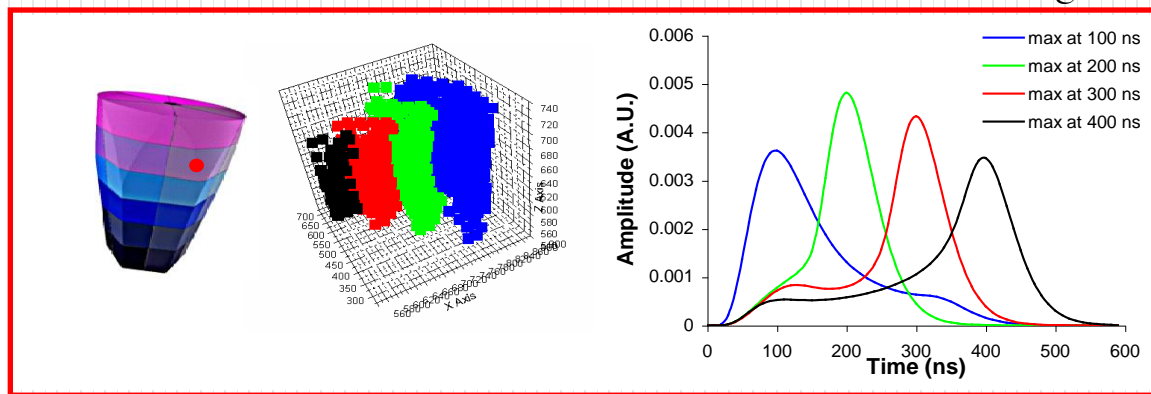
\* F. Recchia, Ph.D Thesis, University of Padova, Italy, 2008.

\*\* F. Recchia, Acta Phys. Pol. B 38 (2007).

\*\*\*" Position resolution of the prototype AGATA triple-cluster detector from an in-beam experiment" F. Recchia, D. Bazzacco, E. Farnea, R. Venturelli, S. Aydin, G. Suliman, C.A. Ur, Nucl. Instr. and Meth. A 604 (2009) 555.

# Recursive Subtraction 3D (RS\_3D) Algorithm

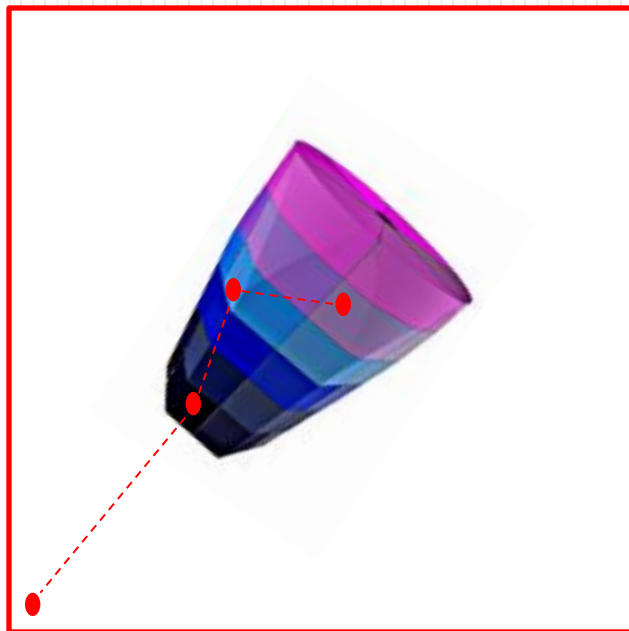
- ❑ The XYZ Position of the interactions is extracted comparing the detector signal shape with reference shapes included in a database (“Signal Basis”).
- ❑ The Signals in the “Basis” are ordered according to specific parameters (e.g. position of the derived net-charge signal maximum) in order to minimize CPU time.
- ❑ For each net charge collecting segment the following operations are performed:
  - the Signals (transients or net charge) which are likely to have a shape that depends on only one interaction are selected.
  - these signals are compared with the Basis elements.
  - the element that best matches is subtracted from the detector signal.



\*“A pulse shape analysis algorithm for HPGe detectors” F.C.L. Crespi, Nucl. Instr. and Meth. A 570 (2007) 459.

\*\*“Application of the Recursive Subtraction Pulse Shape Analysis algorithm to in-beam HPGe signals” F.C.L. Crespi, Nucl. Instr. and Meth. A 604 (2009) 459.

Example: 662 keV\* F.E.P. simulated event\*\*, Segment multiplicity = 3.



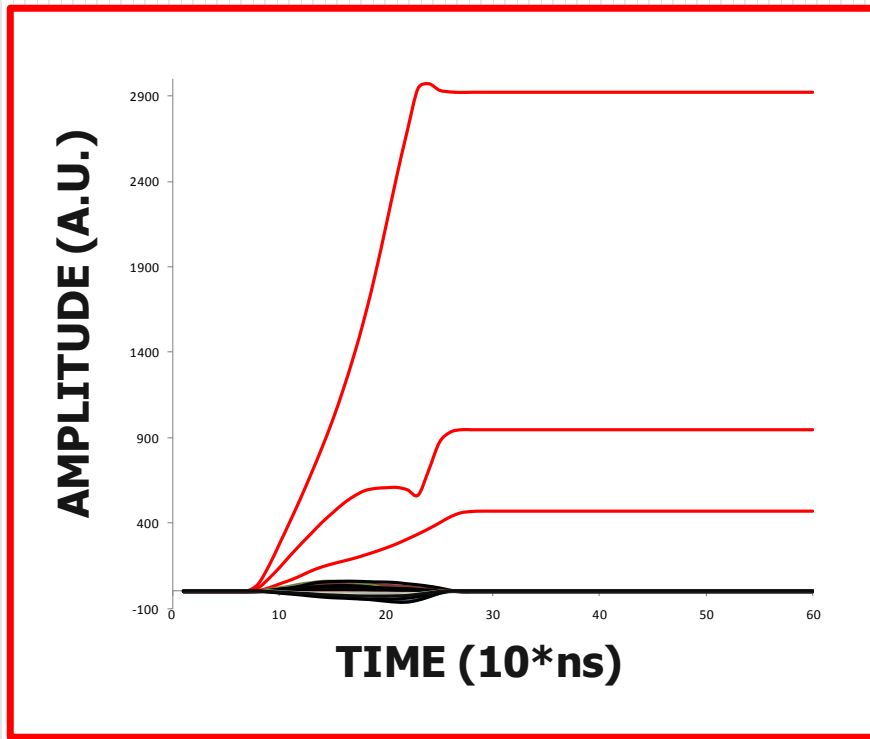
35	5	11	17	23	29	35
34	4	10	16	22	28	34
446 keV		144 keV				
33	3	9	15	21	27	33
32	2	8	14	20	26	32
31	1	7	13	19	25	31
	0	6	12	18	24	30
		72 keV				

\*<sup>137</sup>Cs source, used in tests with experimental data presented in the following.

\*\* Geant 4 AGATA code used

\*\*\* "Conceptual design and Monte Carlo simulations of the AGATA array", E. Farnea et al. NIMA 621 (2010) 331-343 (E. Farnea, D. Bazzacco, LNL-INFN(REP)—202 (2004) 158 website: <http://agata.pd.infn.it>.)

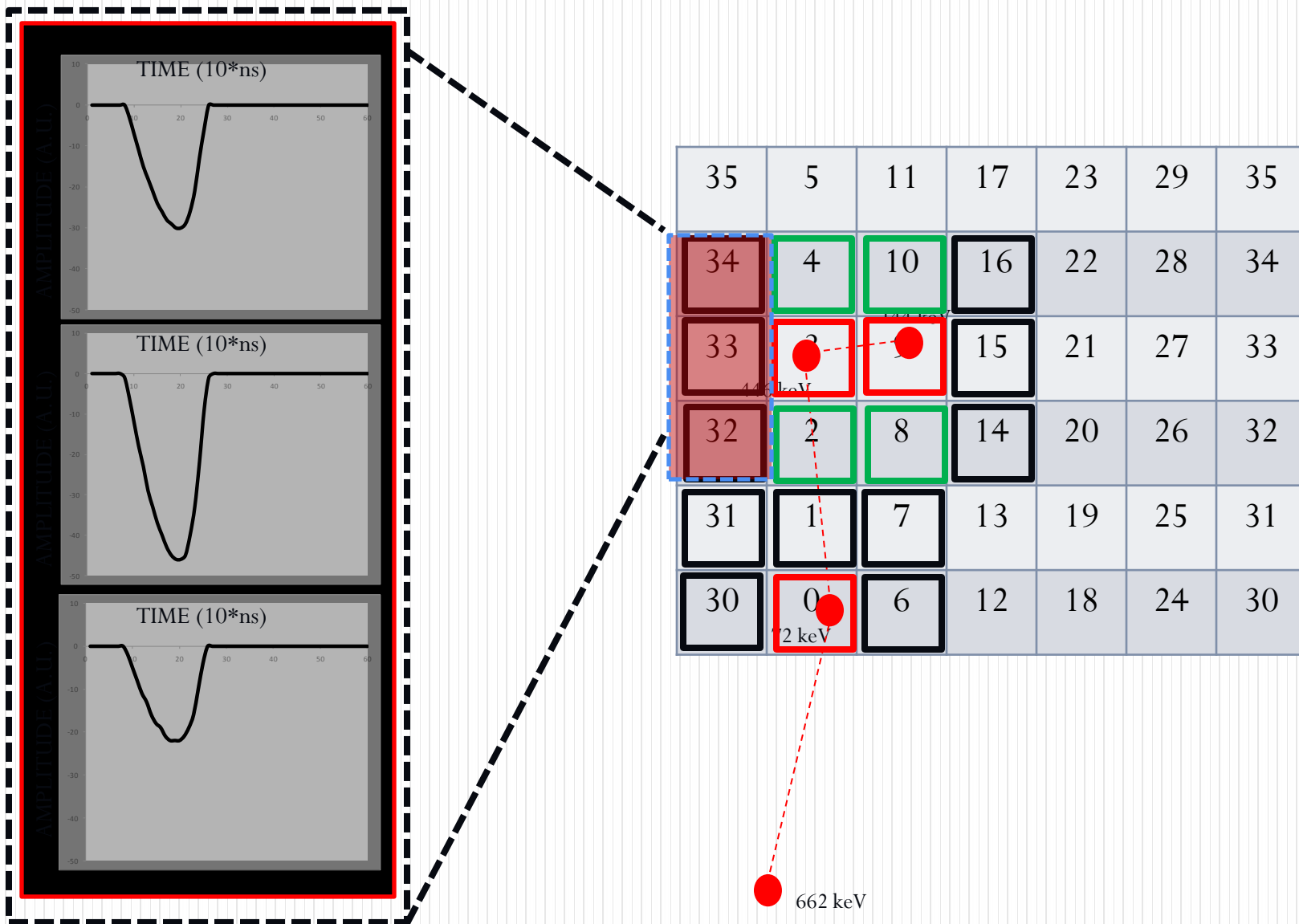
Example: 662 keV F.E.P. simulated event, Segment multiplicity = 3



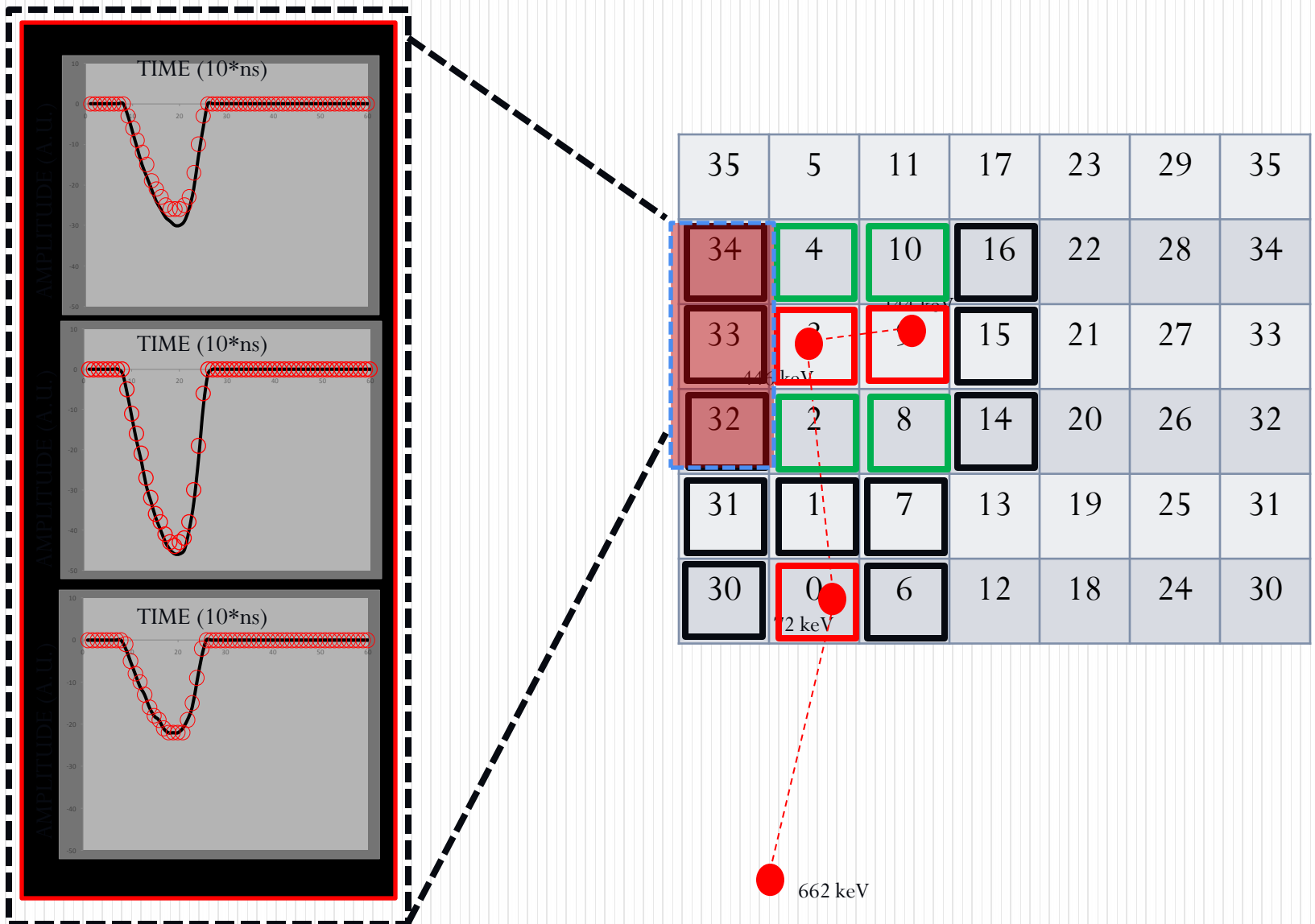
35	5	11	17	23	29	35
34	4	10	16	22	28	34
33	3	9	15	21	27	33
32	2	8	14	20	26	32
31	1	7	13	19	25	31
30	0	6	12	18	24	30

662 keV

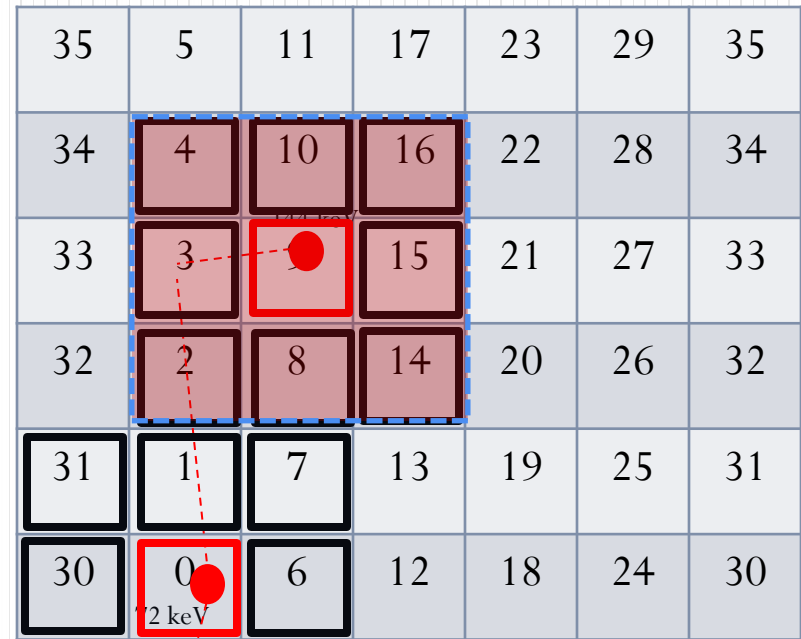
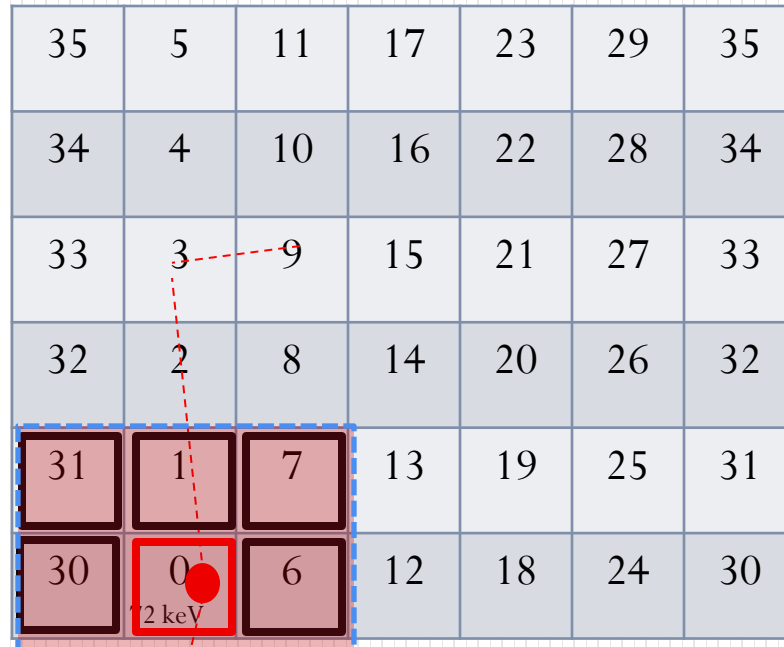
Example: 662 keV F.E.P. simulated event, Segment multiplicity = 3



Example: 662 keV F.E.P. simulated event, Segment multiplicity = 3



Example: 662 keV F.E.P. simulated event, Segment multiplicity = 3

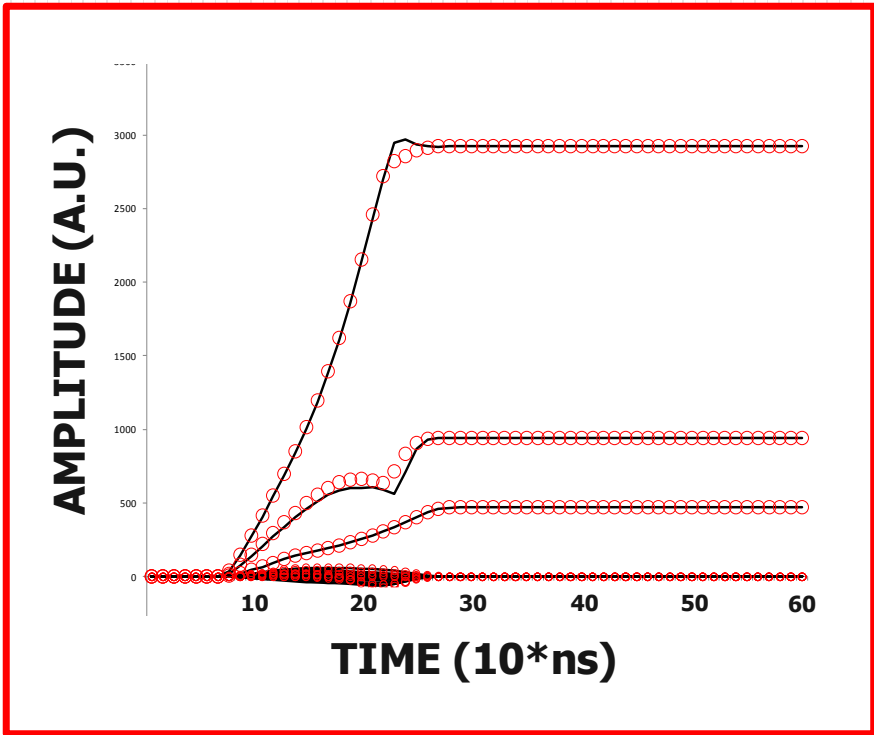


- Net Charge Signals
- Transient Signals  
(1 N.C. segment neighbor only)
- “Superimposed” Transient Signals  
(influenced by multiple N.C. Segments)

● 662 keV

Example: 662 keV F.E.P. simulated event, Segment multiplicity = 3

# Reconstructed Signal



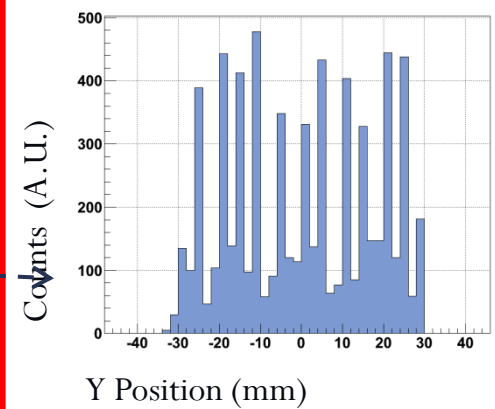
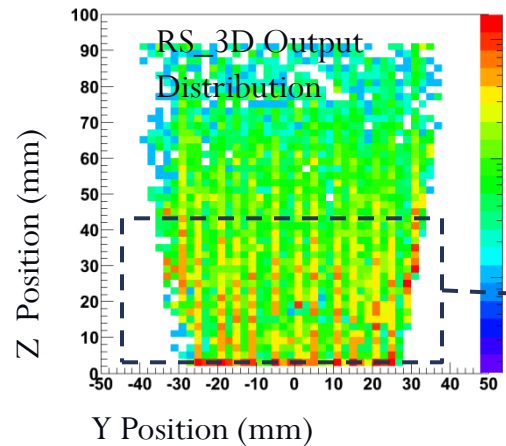
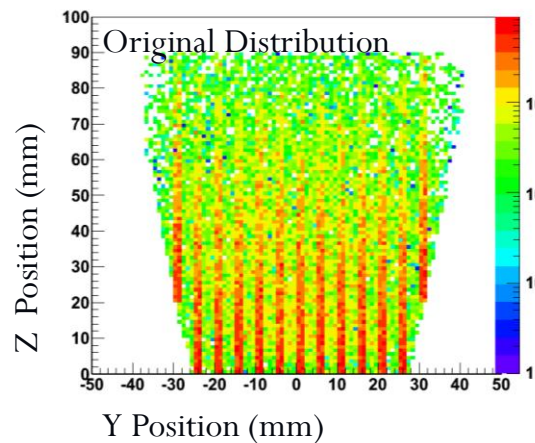
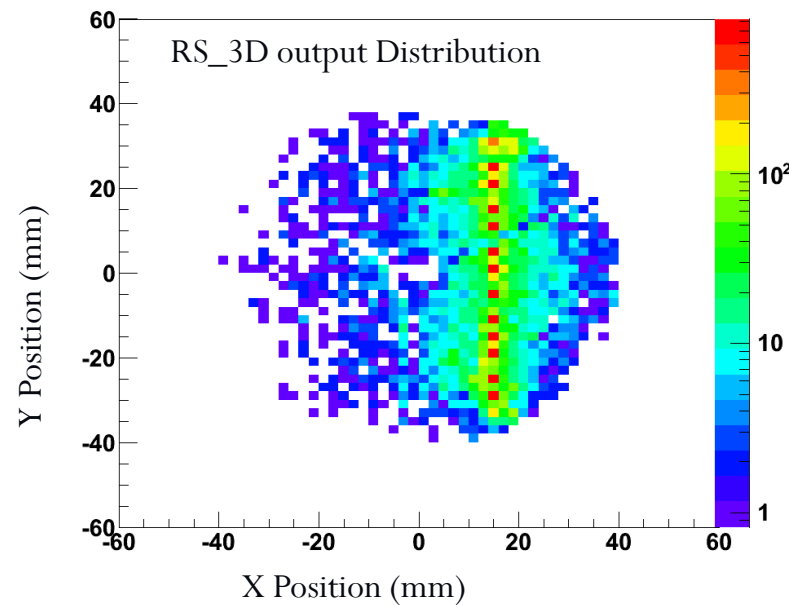
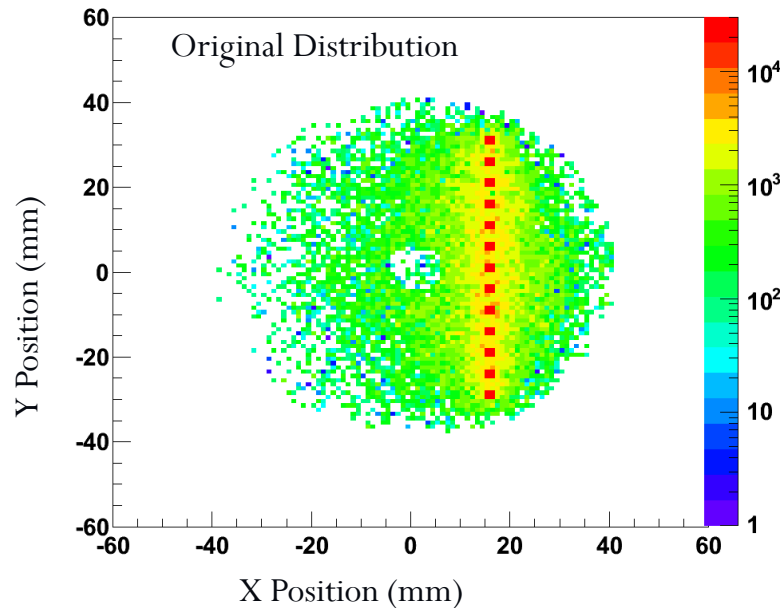
35	5	11	17	23	29	35
34	4	10	16	22	28	34
446 keV		144 keV				
33	3	9	15	21	27	33
32	2	8	14	20	26	32
31	1	7	13	19	25	31
30	0	6	12	18	24	30
		72 keV				

\*\*"A pulse shape analysis algorithm for HPGe detectors" F.C.L. Crespi, Nucl. Instr. and Meth. A 570 (2007) 459. 662 keV

\*\*\*"Application of the Recursive Subtraction Pulse Shape Analysis algorithm to in-beam HPGe signals" F.C.L. Crespi, Nucl. Instr. and Meth. A 604 (2009) 459.

# Pulse Shape Analysis in AGATA

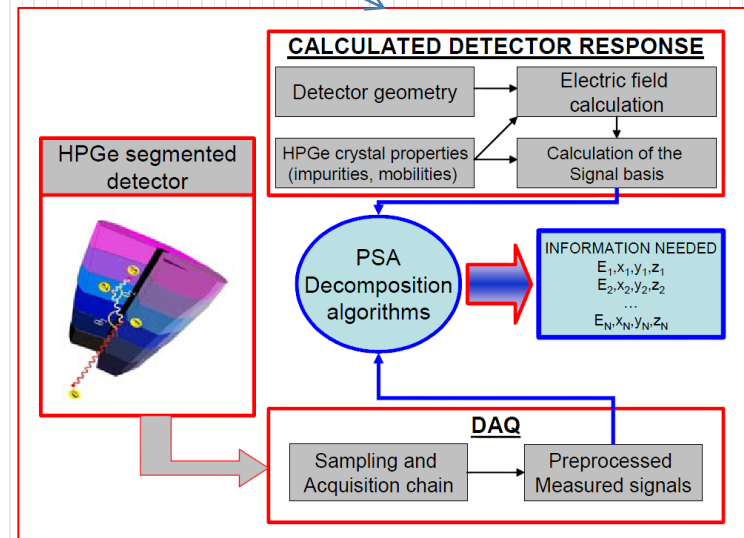
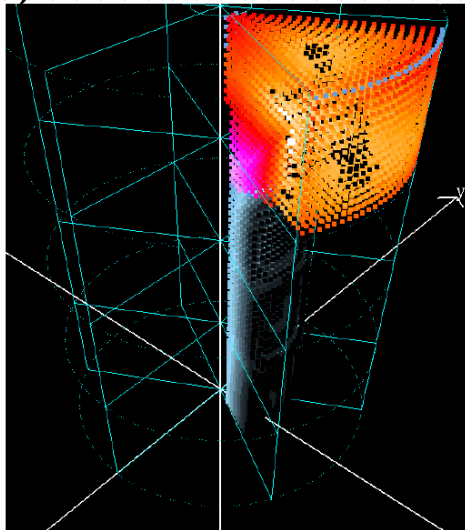
662 keV pencil beam moved along Y direction – 5 mm steps  
(Geant4 + Calculated Signals + preamp response + 5 keV FWHM noise)



# Basis Generation

## Basis Generation

- Most of the PSA algorithms developed for highly segmented HPGe detectors make use of a signal database which contains the detector pulse shapes for all the possible interaction positions inside the detector volume (preamp response, cross talk and other effects have also to be taken into account as well).
- This information is usually extracted calculating the induced current pulses by solving the appropriate electrostatic equations (**→ B. Bruyneel lecture**). **In principle, it is also possible to extract the detector position response experimentally**, but the standard techniques based on coincidence measurements require long time (**→ topic addressed in the next lecture**).
- **Pulse Shape Comparison based Scan (PSCS)**, enormously decreases the time duration of the measurements, allowing a full scan of a large volume HPGe segmented detector in less than 1 week (**→ topic addressed in the next lecture**)
- **differences Experimental basis / Calculated basis (cross talk, preamp response, noise, energy release..)**



Example: **simplified** calculation for the case of a 24-fold cylindrical segmented HPGe detector

The general method to calculate induced charge on electrodes due to the motion of charge carriers in a detector makes use of the Shockley-Ramo theorem<sup>1,2</sup> and the concepts of the *weighting field* and *weighting potential*. The theorem states that the instantaneous current induced on a given electrode is equal to

$$i = q \vec{v} \cdot \vec{E}_0 \quad (\text{D.4})$$

\*

where  $q$  is the charge of the carrier,  $\vec{v}$  is its velocity, and  $\vec{E}_0$  is called the weighting field. Another way of stating the same principle is that the induced charge on the electrode is given by the product of the charge on the carrier multiplied by the difference in the weighting potential  $\varphi_0$  from the beginning to the end of the carrier path:

$$Q = q\Delta\varphi_0 \quad (\text{D.5})$$

To find this weighting potential  $\varphi_0$  as a function of position, one must solve the Laplace equation for the geometry of the detector, but with some artificial boundary conditions:

1. The voltage on the electrode for which the induced charge is to be calculated is set equal to unity.
2. The voltages on all other electrodes are set to zero.
3. Even if a trapped charge is present within the detector volume, it is ignored in the calculation (i.e., the Laplace equation, Eq. (D.2), is used rather than the Poisson equation).

\*G.F. Knoll, Radiation Detection and Measurement, second ed., Wiley, New York, 1989.

### Example: **simplified** calculation for the case of a 24-fold cylindrical segmented HPGe detector

$$i_{ind}(t) = q\vec{E}_{weighting}(\vec{x}(t)) \cdot \vec{v}(\vec{x}(t))$$

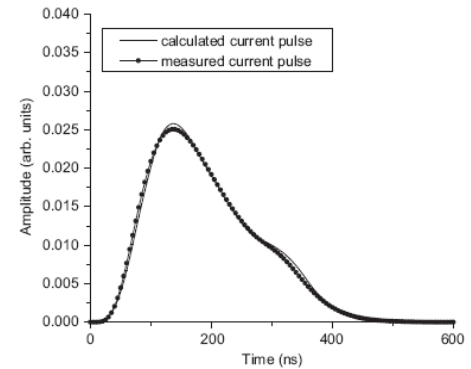
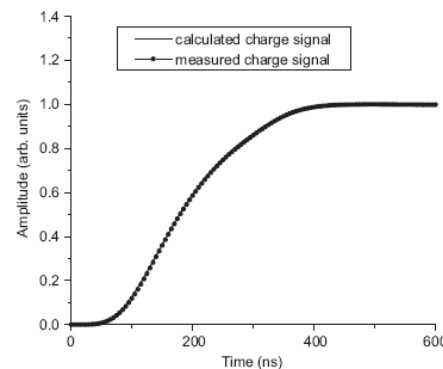
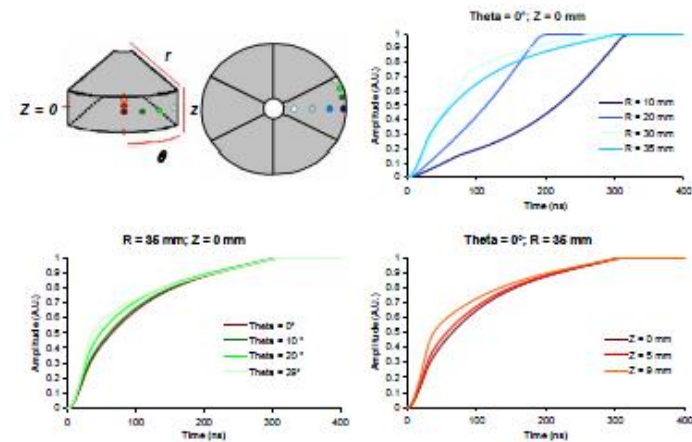
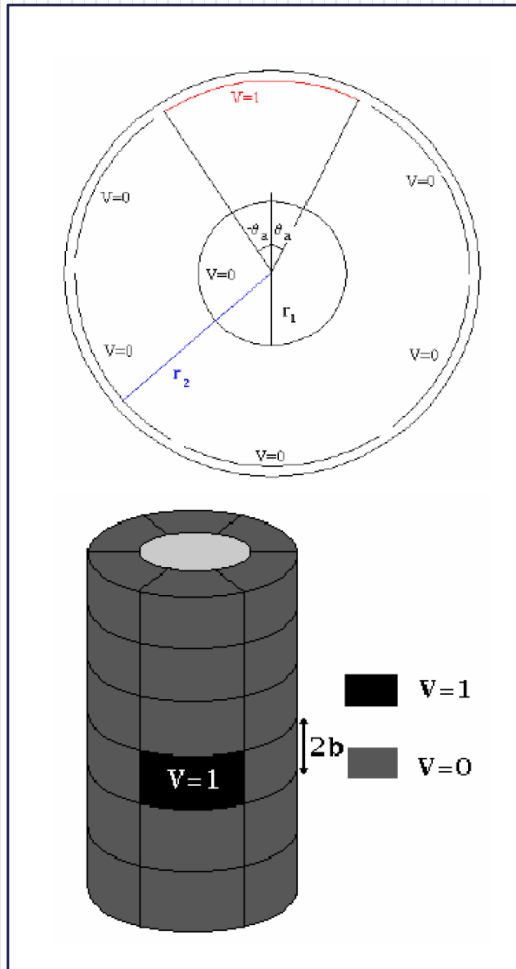
- We need to know the trajectory  $x(t)$  and velocity  $v(x)$  of the charge carriers (electrons and holes) starting from the point in which the  $\gamma$  ray released its energy to the collecting electrode. Since the velocity vector of the charge carriers is determined by the electric field inside the detector we calculate first this quantity.
- We have to compute in each point of the trajectory the charge induced at the electrodes by electrons and holes, this is an electrostatic problem and the solution is obtained solving the equation to find the so called weighting field for the detector geometry of interest.
- Finally we have to put together the previously calculated quantities in order to build the induced current Pulse.  $q$  represents the amount of charge generated following the gamma interaction, therefore it is a quantity proportional to the energy release and it determines the amplitude of the induced charge signal.

**Approximation:** the electric field vector and consequently the charge carriers motion are considered to be parallel to the radial direction. It is not a good approximation when interaction point is close to electrode edges

## Basis Generation

In the case of a 24-fold cylindrical segmented HPGe detector the weighting potential is obtained solving the Laplace equation with the boundary conditions represented in figure and expressed in cylindrical coordinates:

$$\frac{1}{r} \cdot \frac{d}{dr} \left( r \frac{dV}{dr} \right) + \frac{1}{r^2} \cdot \frac{d^2V}{d\theta^2} + \frac{d^2V}{dz^2} = 0$$



\*P. Pulici; Graduation Thesis, Politecnico di Milano, 2004.

## Analytical solution of the weighting potential and weighting field for a 24 fold segmented cylindrical HPGe detector

The analytical form for the weighting potential  $V_{\text{peso}}(r, \theta, z)$  is reported in the following [88]:

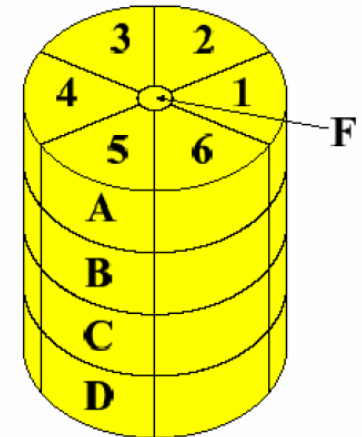
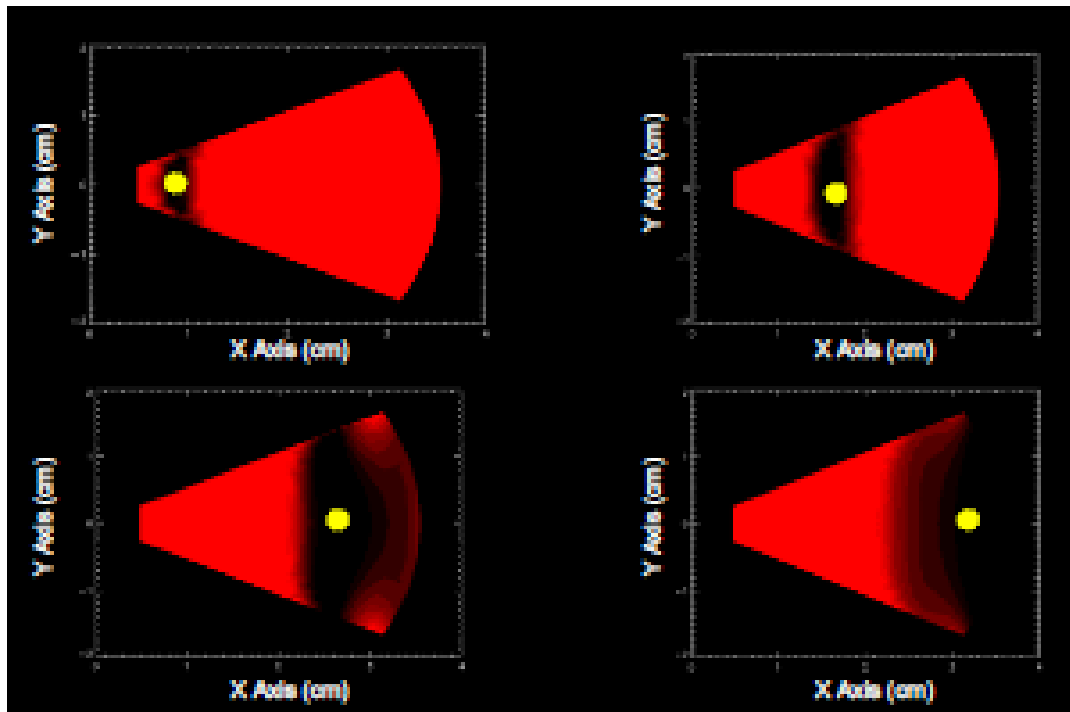
$$\begin{aligned}
 V_{\text{peso}}(r, \theta, z) &= \\
 &= \frac{2}{\pi \cdot B} \cdot \vartheta_a \cdot b \cdot \frac{1}{\log\left(\frac{r}{r_1}\right)} \cdot \log\left(\frac{r}{r_1}\right) + \\
 &+ \sum_{\substack{m_z \neq 0 \\ (m_z=0)}} \frac{4}{\pi \cdot B} \cdot \vartheta_a \cdot \frac{\text{sen}(m_z \cdot b)}{m_z} \cdot \cos(m_z \cdot z) \cdot \frac{K_0(m_z \cdot r_1) \cdot I_0(m_z \cdot r) - I_0(m_z \cdot r_1) \cdot K_0(m_z \cdot r)}{K_0(m_z \cdot r_1) \cdot I_0(m_z \cdot r_2) - I_0(m_z \cdot r_1) \cdot K_0(m_z \cdot r_2)} \\
 &+ \sum_{\substack{m_\theta \neq 0 \\ (m_\theta=0)}} \frac{4}{\pi \cdot B} \cdot \frac{\text{sen}(m_\theta \cdot \vartheta_a)}{m_\theta} \cdot b \cdot \cos(m_\theta \cdot \theta) \cdot \frac{\left[\left(\frac{r}{r_1}\right)^{m_\theta} - \left(\frac{r_1}{r}\right)^{m_\theta}\right]}{\left[\left(\frac{r_2}{r_1}\right)^{m_\theta} - \left(\frac{r_1}{r_2}\right)^{m_\theta}\right]} \\
 &+ \sum_{m_\theta \neq 0} \sum_{m_z \neq 0} \frac{8}{\pi \cdot B} \cdot \frac{\text{sen}(m_\theta \cdot \vartheta_a)}{m_\theta} \cdot \frac{\text{sen}(m_z \cdot b)}{m_z} \cdot \cos(m_\theta \cdot \theta) \cdot \cos(m_z \cdot z) \cdot \frac{K_{m_\theta}(m_z \cdot r_1) \cdot I_{m_\theta}(m_z \cdot r) - I_{m_\theta}(m_z \cdot r_1) \cdot K_{m_\theta}(m_z \cdot r)}{K_{m_\theta}(m_z \cdot r_1) \cdot I_{m_\theta}(m_z \cdot r_2) - I_{m_\theta}(m_z \cdot r_1) \cdot K_{m_\theta}(m_z \cdot r_2)}
 \end{aligned}$$

The analytical form for the radial component of weighting field vector  $E_{\text{peso}}(r, \theta, z)$  is reported

$$\begin{aligned}
 E_{r,\text{peso}}(r, \theta, z) &= \frac{2}{\pi \cdot B} \cdot \vartheta_a \cdot b \cdot \frac{1}{\log\left(\frac{r}{r_1}\right)} \cdot \frac{1}{r} + \\
 &+ \sum_{\substack{m_z \neq 0 \\ (m_z=0)}} \frac{4}{\pi \cdot B} \cdot \vartheta_a \cdot \frac{\text{sen}(m_z \cdot b)}{m_z} \cdot \cos(m_z \cdot z) \cdot \frac{m_z \cdot [K_0(m_z \cdot r_1) \cdot I_1(m_z \cdot r) + I_0(m_z \cdot r_1) \cdot K_1(m_z \cdot r)]}{K_0(m_z \cdot r_1) \cdot I_0(m_z \cdot r_2) - I_0(m_z \cdot r_1) \cdot K_0(m_z \cdot r_2)} \\
 &+ \sum_{\substack{m_\theta \neq 0 \\ (m_\theta=0)}} \frac{4}{\pi \cdot B} \cdot \frac{\text{sen}(m_\theta \cdot \vartheta_a)}{m_\theta} \cdot b \cdot \cos(m_\theta \cdot \theta) \cdot m_\theta \cdot \frac{\left[\frac{1}{r_1} \cdot \left(\frac{r}{r_1}\right)^{m_\theta-1} + \frac{1}{r} \cdot \left(\frac{r_1}{r}\right)^{m_\theta}\right]}{\left[\left(\frac{r_2}{r_1}\right)^{m_\theta} - \left(\frac{r_1}{r_2}\right)^{m_\theta}\right]} \\
 &+ \sum_{m_\theta \neq 0} \sum_{m_z \neq 0} \frac{8}{\pi \cdot B} \cdot \frac{\text{sen}(m_\theta \cdot \vartheta_a)}{m_\theta} \cdot \frac{\text{sen}(m_z \cdot b)}{m_z} \cdot \cos(m_\theta \cdot \theta) \cdot \cos(m_z \cdot z) \cdot \\
 &\cdot \frac{1}{K_{m_\theta}(m_z \cdot r_1) \cdot I_{m_\theta}(m_z \cdot r_2) - I_{m_\theta}(m_z \cdot r_1) \cdot K_{m_\theta}(m_z \cdot r_2)} \cdot \\
 &\left[ K_{m_\theta}(m_z \cdot r_1) \cdot \left( m_z \cdot I_{m_\theta-1}(m_z \cdot r) - \frac{m_\theta}{r} \cdot I_{m_\theta}(m_z \cdot r) \right) + \right. \\
 &\left. + I_{m_\theta}(m_z \cdot r_1) \cdot \left( m_z \cdot K_{m_\theta-1}(m_z \cdot r) + \frac{m_\theta}{r} \cdot K_{m_\theta}(m_z \cdot r) \right) \right]
 \end{aligned}$$

\*P. Pulici; Graduation Thesis, Politecnico di Milano, 2004.

- **25-fold segmented MARS HPGe detector segment section in the X,Y plane is shown**
- *The similarity in shape between a net charge signal associated with a single interaction in a fixed position (indicated in each panel by a yellow dot) is evaluated, by means of a  $\chi^2$  comparison, with the signals for all the other possible positions in the segment.*
- The more the region is “red”, the larger is the  $\chi^2$  value; on the contrary black colored regions are associated with signals that have very similar shape as compared to the one in the position indicated by yellow dot.



Layout of the MARS segmentation.

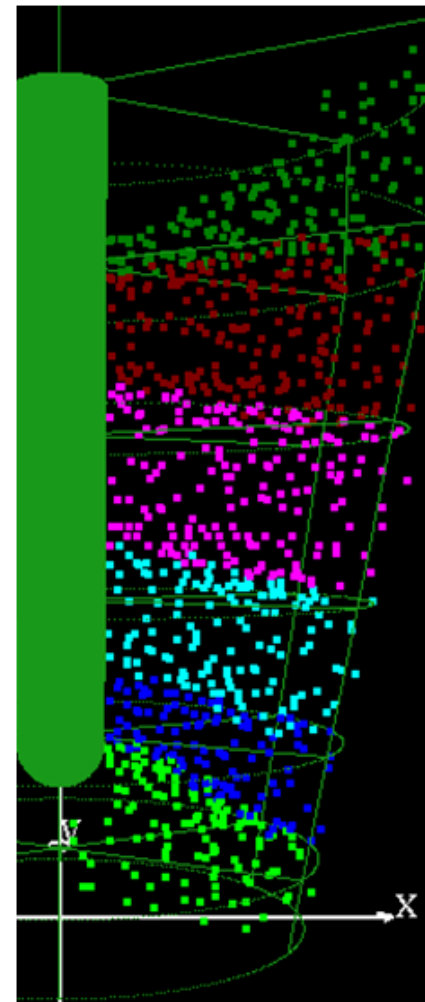
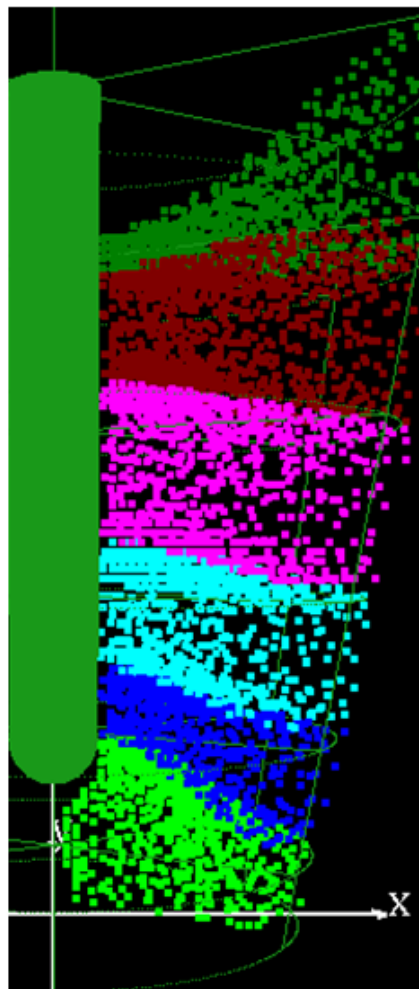
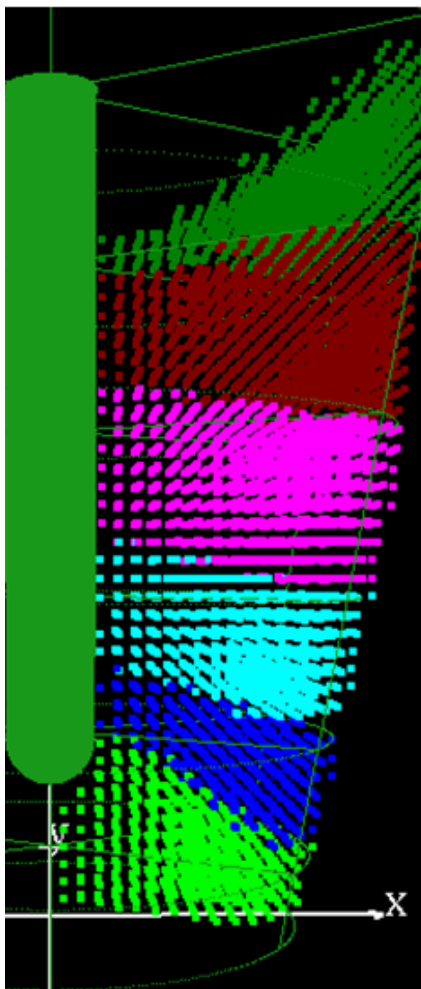
- Th. Kröll, D. Bazzacco, “Simulation and analysis of pulse shapes from highly segmented HPGe detectors for the g-ray tracking array MARS”, NIMA 463 (2001) 227-249.
- Th. Kröll, D. Bazzacco, “ A genetic algorithm for the decomposition of multiple hit events in the  $\gamma$ -ray tracking detector MARS””, NIMA 565 (2006) 691-703
- Th. Kröll et al., “In-beam experiment with the  $\gamma$ -ray tracking detector MARS”, NIMA 586 (2008) 421-431

# Tests with grids: regular and irregular

Base2mm

xyz\_chi2\_1E7\_d5

xyz\_chi2\_5E7\_d5



\* R. Venturelli presentations at AGATA weeks (e.g. Liverpool June 2006) available at at [http://www-win.gsi.de/agata/](http://www.win.gsi.de/agata/)

\*\* R. Venturelli, et al., LNL Annual Report 2002, INFN-LNL(REP)198/2003, pp. 154–156



34416



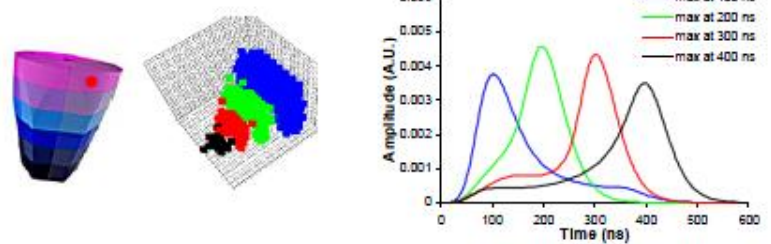
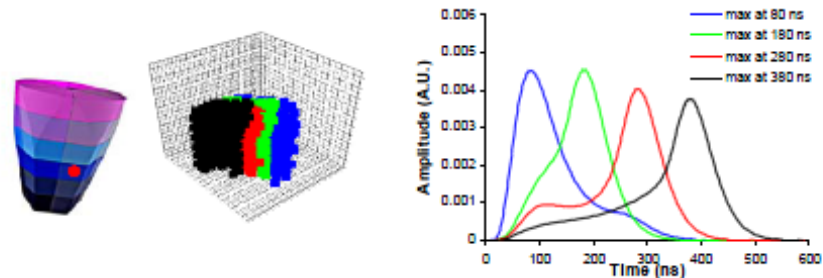
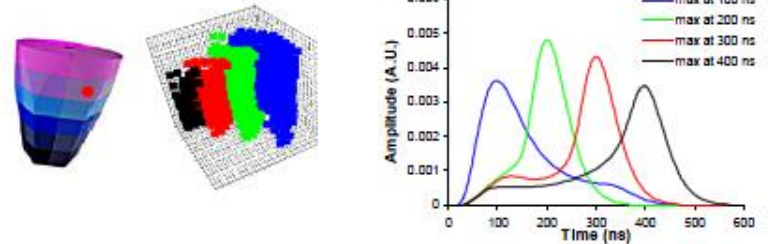
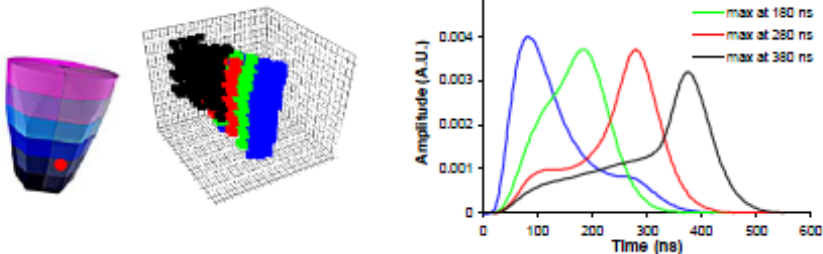
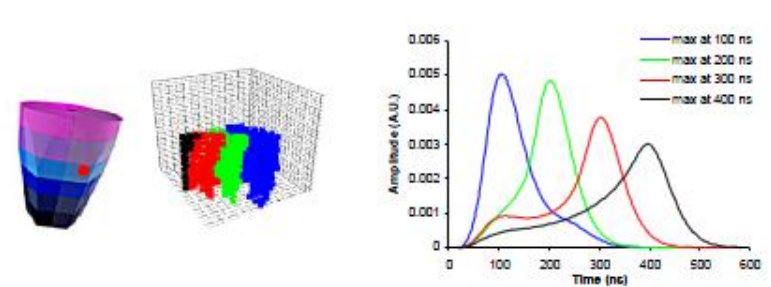
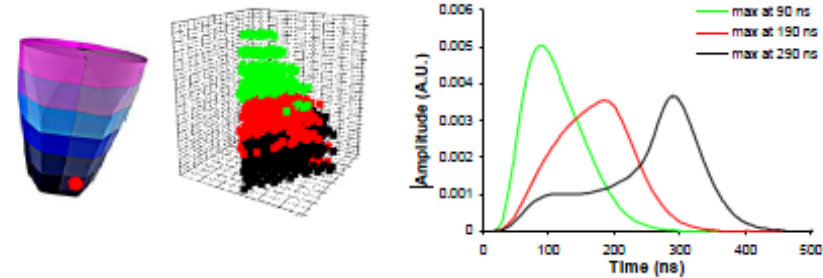
26391



4164

## Basis Generation

Each panel displays an AGATA geometry crystal where the selected segment is labeled with a red dot; the grid points of (MGS\*) basis for the same segment are plotted in different colors depending on the position of the current pulse maximum and finally a set of current pulses representative of each “colored zone” is plotted



\*P.Medina, et al., A Simple Method for the Characterization of HPGe Detectors, IMTC 2004, Como, Italy, website: <http://mgs2005.in2p3.fr/Mgs.phpS>.